Current deformation of the Digne Nappe (southwestern Alps) from a comparison between triangulation and GPS data

François Jouanne, J. C. Hippolyte, J. F. Gamond, J. Martinod

Geophys. J. Int. (2001) **144,** 432–440

Current deformation of the Digne Nappe (southwestern Alps) from a comparison between triangulation and GPS data

François Jouanne,[1] J. C. Hippolyte,[1] J. F. Gamond[2] and J. Martinod[2]

[1] *Laboratoire de Geodynamique des Chaines Alpine, University de Savoie, Campus Scientifique, UMR CNRS* 5025, 73376 *Le Bourget du Lac Cedex, France. E-mail: jouanne@univ-savoie.fr*

[2] *LGIT, UMR CNRS* 5559, *Université J. Fourier,* BP 53X, 38041 *Grenoble Cedex* 9, *France*

Accepted 2000 September 20. Received 2000 September 11; in original form 2000 January 24

SUMMARY

The negligible present-day convergence between northern Italy and stable Europe as shown by continuous GPS measurements and the low level of Alpine seismicity both indicate that present-day deformation in the western Alps is very moderate. Nevertheless, from historical seismicity records, the Moyenne Durance Fault can be identified as an active structure, and a brief neotectonic and geomorphological analysis indicates that Plio–Quaternary deformation occurred in the northern Valensole Basin and in the Digne Nappe. A comparison is made between 1949 and 1952 triangulation data and 1997 GPS data to estimate the current deformation in the Digne Nappe and around the Moyenne Durance Fault in the southwestern Alps. The deformation is represented by the maximum angular shear rates needed to make the characterization of the deformation independent of the rigid rotation and scale effects that are introduced in the velocity field when using triangulation data. Errors on maximum angular shear rates are simulated using a Monte Carlo analysis of the errors of the triangulation data. The main results are: (1) the existence of moderate deformation in the inner part of the Digne Nappe; (2) deformation of the northern Valensole Basin; (3) significant deformation in the southern part of the Moyenne Durance Fault; and (4) a lack of measurable deformation in the southern Valensole Basin–Provencale range area and south of the Lure Mountain.

Key words: collision belts, continental deformation, geodesy, satellite geodesy, tectonics.

INTRODUCTION

Determination of the present-day deformation between the Digne Nappe and the Valensole Basin and along the Moyenne Durance Fault is essential in order to understand the present-day tectonics of the southwestern Alps. In this study, an attempt is made to determine the present-day deformation and to test its continuity with Mio–Pliocene deformation as estimated according to previous studies. In particular, present-day deformation is tested to see whether it is located along the Digne Nappe thrust fault, along a blind thrust in the northern Valensole Basin or in the inner part of the Nappe, thus involving an out-of-sequence process. In addition, the present-day tectonics are analysed to see whether they show a significant change in the shortening direction like the Miocene tectonics, which change from E–W shortening west of the Pelvoux External Crystalline Massif to N–S shortening in the southern Alps. Present-day deformation is estimated by several methods: comparison between triangulation and GPS data (Fig. 1) to estimate horizontal deformation, and focal mechanism and tectonic data analyses.

GEOLOGICAL FRAMEWORK

The study area is located at the front of the outermost Alpine Nappe, the Digne Nappe (Figs 2 and 3), forming the southern part of the external arc of the western Alps. The northern part of this area is located just southwest of the southwestern end of the Pelvoux External Crystalline Massif, where the Miocene shortening directions changed from E–W north of this limit, in the Vercors Subalpine Massif, to N–S south of it, in the Digne Nappe and in the Castellane and Nice arcs.

The Digne Nappe was emplaced on a Triassic evaporitic sequence during the late Alpine convergence (late Eocene to Mio–Pliocene, e.g. Lickorish & Ford 1998) and was probably still moving during Quaternary times (Clauzon 1975; Jorda *et al.* 1992). In this nappe, the analysis of fault plane kinematics indicates global NE–SW directions of compression (Combes 1984; Lickorish & Ford 1998), but these directions may have changed with time from NE–SW to NNE–SSW (Ritz 1992) or from NNE–SSW to ENE–WSW (Faucher *et al.* 1988). This latter trend seems to be confirmed by the analysis of Pliocene and Quaternary alluvial deposit deformation (Hippolyte &

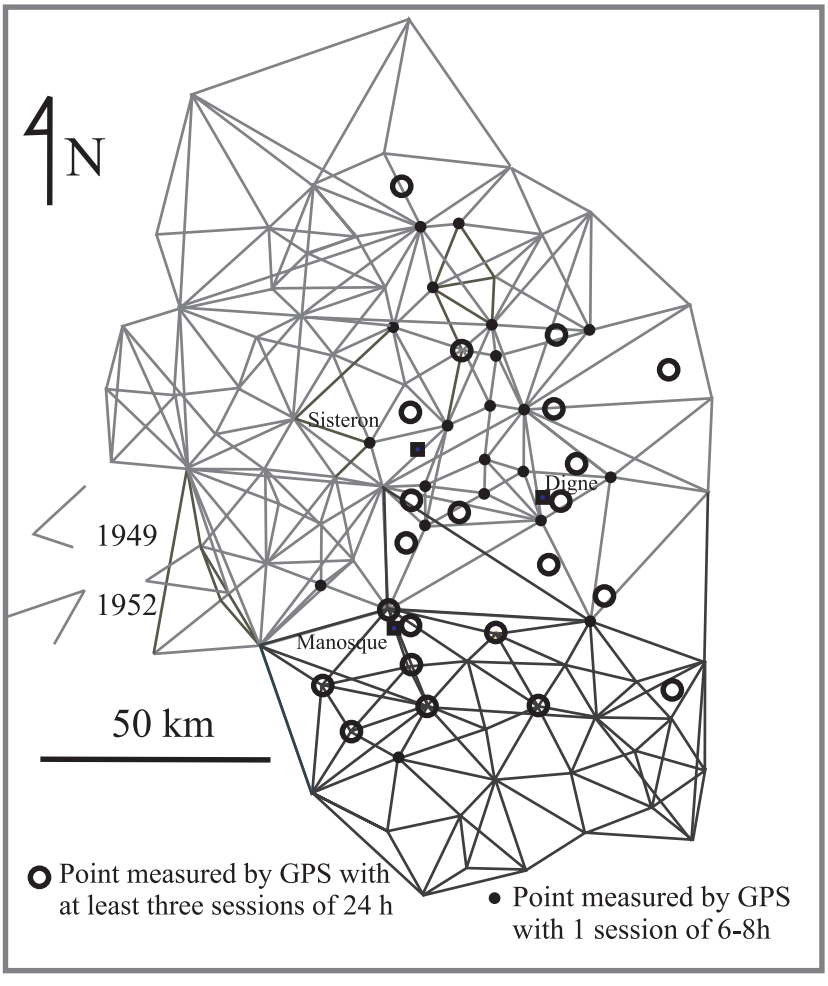

Figure 1. First- and second-order triangulation network performed by the Institut Géographique National in 1949 and in 1952, with the locations of the benchmarks measured by GPS in 1997.

Jouanne 1998). Near the town of Digne, this nappe overthrusts the Neogene succession of the Valensole Basin, which is itself folded with E–W to NNW–SSE fold axes in its northern part (Haccard *et al*. 1989). The easternmost part of the nappe stack is currently undergoing E–W extension at depth, as shown by the stress axis determined from the inversion of focal mechanisms (Sue *et al*. 1999).

The western margin of the Valensole Basin corresponds to the Moyenne Durance Fault (Fig. 3), a probable fracture in the Hercynian basement that was reactivated with west-side-up motion during the late Miocene (e.g. Roure *et al*. 1992) and is still active in its southern part (near the town of Manosque), where several intensity VIII earthquakes in 1509, 1708, 1812 and 1913 (Lambert *et al*. 1996) are known to have occurred. The tectonic structures along this fault indicate that it operated with a reverse sense and a sinistral component during the Miocene (Terrier 1991), which was confirmed by the determination of NW–SE to NNE–SSW directions of compression (Combes 1984; Bergerat 1985; Terrier 1991; Ritz 1992). Its present movement is assumed to be still the same as during Miocene times (e.g. Ritz 1992).

ESTIMATING HORIZONTAL DEFORMATION

Triangulation data

Triangulation observations (Fig. 1) were carried out to build the first- and second-order national geodetic reference network in this area. As a consequence, the configuration of the network is not optimal for geophysical investigations: for instance, there are few benchmarks around the Moyenne Durance Fault zone where periodic activity is known to occur, indicated by its regular historical seismicity.

The triangulation network was observed in 1949 (Préalpes 1949) and 1952 (Provence 1952) by the IGN (Institut Géographique National). The measurements were performed with Wild T3 theodolites with reiteration of the measurements 8–32 times. The two networks (1949 and 1952) are connected by five common geodetic benchmarks with common direction observations. The triangulation network includes 629 direction measurements and 79 geodetic sites. Several types of benchmarks were used: IGN or SGA granite markers with a cross

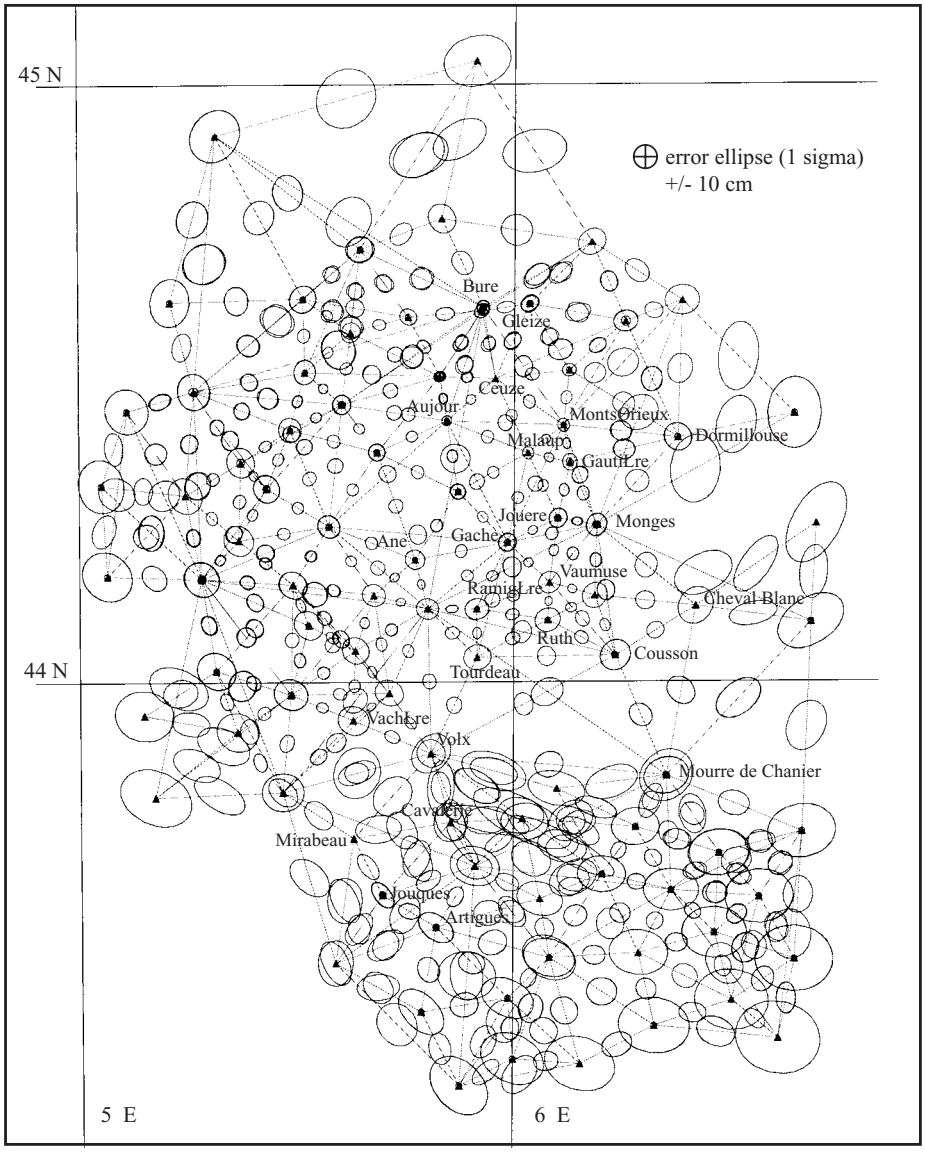

Figure 2. Triangulation network used in this study (1949–1952) with 1σ error ellipses scaled by the variance factor. Error ellipses are drawn on the coordinates and between connected points.

engraved at the bottom and brass benchmarks directly embedded in the rock (generally massive calcareous formations in this area). A reconnaissance field trip was carried out by two geologists to check whether the points were still in the geodetic site and also to assess benchmark stability.

It was considered that the standard deviations of the triangulation observations are a function of centring errors and random instrumental errors. The standard deviation of a direction measurement was assumed to be

$$\sigma_V = \sqrt{k(A/D)^2 + (B/\sqrt{n})^2}, \quad (1)$$

where σ_V is expressed in 10^{-4} grads, D is the distance between the theodolite and the rod in km, n is the number of reiterations of the measurement, and A and B are, respectively, the standard deviation of the centring and the standard deviation of the instrument error (according to IGN studies). A is expressed in mm, B in 10^{-4} grads and $k=[(400\times10^{-2})/(2\pi)]^2$ converts mm^2 to $(10^{-4}$ grads$)^2$. In this study, a centring error of $A=20$ mm was considered (representing the centring error of the theodolite and the rod) and a standard deviation of the Wild T3 theodolite of $B=3.5\times10^{-4}$ grads.

The triangulation data were adjusted with the Geolab V2.4 software taking the GPS coordinates of remeasured points as *a priori* coordinates and, for the other points, coordinates with ellipsoidal height determined from their altitude and corrected using a geoid grid (Duquenne 1997, 1998). The vertical deflection components for each point were estimated from the local slopes of the quasi-geoid model QGF98 (Duquenne 1997, 1998). To make the observations as homogeneous as possible, the measurements between different points of a geodetic site were replaced by coordinate differences between the various benchmarks (if the distance between benchmarks was less than 10 m). When the distance between the points exceeded 20 m or when the tie-in measurements were ambiguous, these measurements were reobserved by GPS wherever possible. When this was impossible

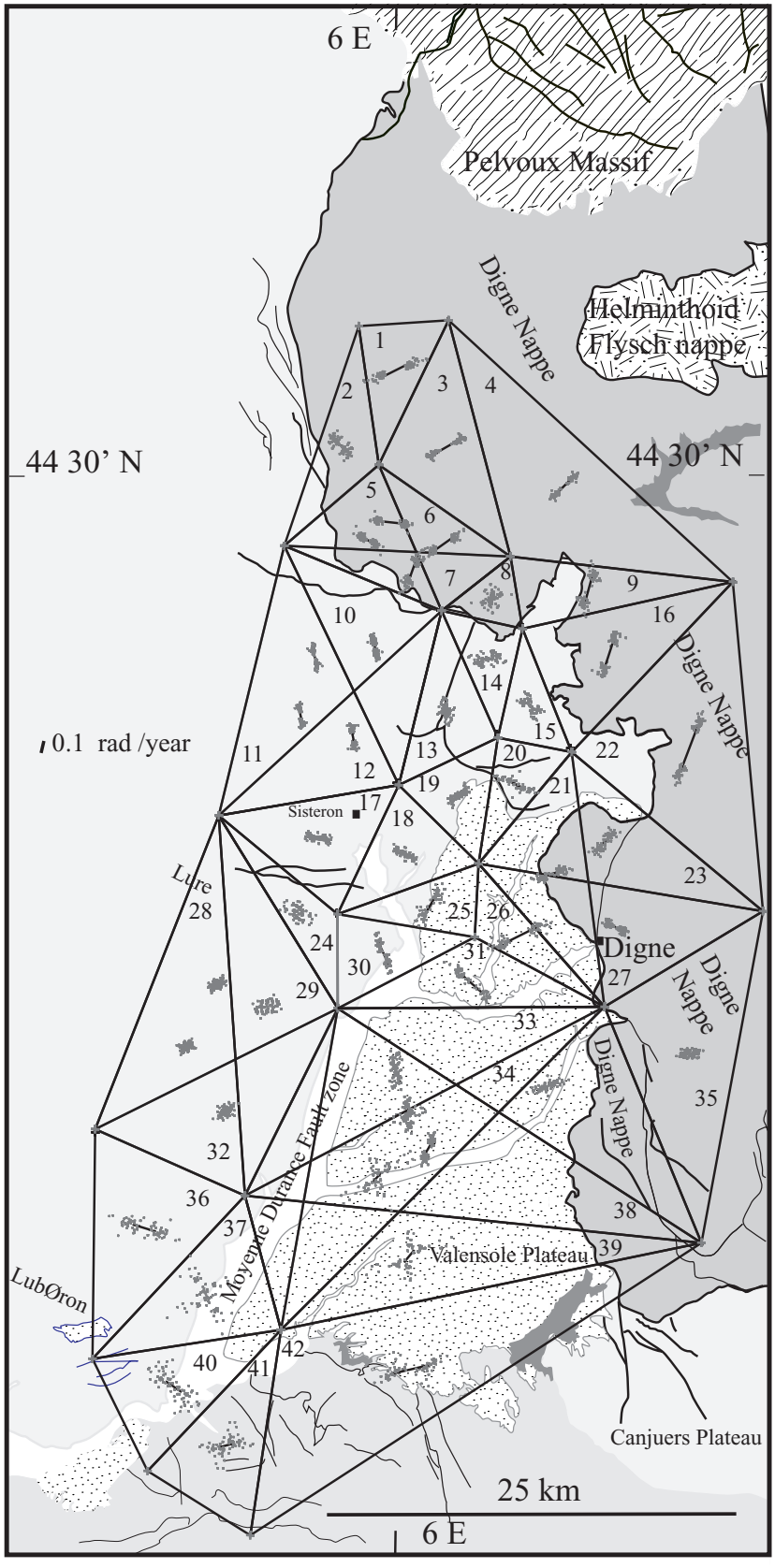

Figure 3. Maximum angular shear rates drawn in the maximum compression direction. The maximum angular shear strain rates are drawn in the barycentres of the triangles used for their determination and tested with a Monte Carlo error analysis. The dispersion of points represents the errors for a 1σ confidence level scaled by the variance factor estimated from the undisturbed triangulation data set.

(for example, when the point was in a church tower), the site was excluded from the deformation estimation. Observation errors were tracked down by examining the differences between observed and calculated values (adjustment residuals). Fig. 2 represents the adjusted network with 1σ error ellipses scaled by the variance factor. Relative confidence ellipses between connected points were also drawn, these ellipses being probably more representative of uncertainties for an angular shear rate estimated in triangles with apices formed by adjacent points. The mean uncertainty between the triangulation points is 3.6 ppm.

GPS data

During summer 1997, triangulation benchmarks were remeasured using dual-frequency Ashtech GPS receivers. Two kinds of measurements were performed (Fig. 1): (1) easily accessible old points and new points were measured over a period of at least three days to enable future calculations of deformation using only comparisons between GPS data, and (2) points located on the Alpine summits, generally a few kilometres from the first category of points, were determined with one session of 6–8 hr. All the data were analysed with the Bernese V4.0 software in the ITRF94 reference frame, using IGS precise orbits and IGS Earth Orientation Parameters and data from continuous GPS stations at Zimmerwald (Switzerland), Grasse (France), Graz (Austria), Hersmontceux (England), Villafranca (Spain), Torino, Matera, Noto and Cagliari (Italy). The antenna phase centre offsets and the phase centre variations as a function of the elevation were corrected with a calibration file. To increase the vertical-component accuracy, troposphere parameters were estimated. One normal equation per session was obtained, the final solution being estimated with the addition of all the normal equations.

Points located on the Alpine summits were measured during one session of 6–8 hr and it was thus impossible to compute the short-term repeatability for these points. To estimate the uncertainties on these points, the 24 hr sessions of the precise points measured were cross-referenced with several 24 hr sessions in four sessions of 6 hr per day. The values of these short-term repeatabilities of the horizontal component were always less than 7 mm. It was assumed that this value is representative of the horizontal uncertainties of the points measured with only one 6–8 hr session, which is good enough to perform a deformation study with data measured 50 years previously.

Deformation estimation

The major difficulty when estimating deformation stems from the difference between the nature of the two types of measurements. Triangulation measurements can be used to obtain the values of all the angles in any triangular mesh of the network, but not to determine the distances between nodes (apices of the triangles). Thus, the shape of any triangle is known but its size can only be estimated to within a scale factor. To adjust the network and give it a scale and orientation, a distance and an azimuth must be known, for example, when two points are fixed to their *a priori* GPS coordinates. Conversely, GPS measurements provide a means of estimating the geocentric coordinates of the points in the network calculated with reference to continuous IGS stations defining a specific reference system (ITRF94 here). Therefore, the shape and also the size and orientation of the triangles, and thus of the whole network, are known.

When the measurements of the two epochs are to be compared, two points of the triangulation network are selected and are given the coordinates as calculated by GPS. The scale and orientation of the network are thus fixed arbitrarily. However, if a relative displacement between these two points occurs during the time span between the triangulation and the GPS measurement campaigns, the displacement field is affected by a scale effect and a rigid deformation. Therefore, in such a comparison, several deformation components cannot be determined: rigid body rotation of the network, translation and dilatation. Conversely, the distortion component of strain can be calculated applying Frank's (1966) method, reused by Feigl *et al.* (1990), Reilly & Gubler (1990), Jouanne *et al.* (1994) and Ferhat *et al.* (1998).

The aim of this method is to calculate the distortion component of the infinitesimal strain tensor in every triangle and to extract from this component the value of the maximum angular shear strain, γ, and the azimuth, ψ, of the minor principal axis of infinitesimal strain. These elements can be calculated from the changes in the angles ($\delta\phi_a$, $\delta\phi_b$, $\delta\phi_c$) in every triangle.

The maximum angular shear strain, γ, is the value of the greatest change in the angle between two lines that were initially perpendicular in the undeformed state (Ramsay 1967; Ramsay & Huber 1983; Jaeger 1978). In a 2-D Cartesian reference frame with N–S and E–W axes, the infinitesimal distortion is shown to result from the combination of two angular shear strains, γ_1 and γ_2. The total angular shear strain is

$$\gamma = (\gamma_1^2 + \gamma_2^2)\,. \tag{2}$$

The significance of these quantities and their combinations is sketched in Fig. 4 (see also Feigl *et al.* 1990, Fig. 6). γ_1 corresponds to the angular shear strain of lines oriented NE–SW and NW–SE, and γ_2 to that of N–S and E–W lines. The infinitesimal strain theory states that the maximum angular shear strain (γ_1) of NE–SW and NW–SE lines can be achieved if one of the principal axes of the strain ellipse is oriented N–S, that is, either through the pure shear of a N–S or E–W shortening axis, or through the simple shear of a NE–SW or NW–SE shear direction. Similarly, the maximum angular shear strain (γ_2) of N–S and E–W lines can be achieved if one of the principal axes of the strain ellipse is oriented NE–SW, through pure shear with a NE–SW or NW–SE shortening axis or simple shear with an E–W or N–S shear direction. Knowing γ_1 and γ_2, it is then possible to calculate the azimuth, ψ, of the principal shortening axis of the infinitesimal strain ellipse,

$$\tan 2\psi = (\gamma_1/\gamma_2)\,. \tag{3}$$

The continuum mechanics theory states that the minor principal axis of the infinitesimal strain ellipse is parallel to the major principal stress (σ_1) direction. In seismotectonic studies the direction of the major principal stress, σ_1, that generated a seismic event (P-axis) is assigned to the tension quadrant and assumed to be in the compressional diedron defined by the two nodal planes of the focal sphere. When σ_1 and σ_3 are horizontal, the traces of the nodal planes can therefore be superimposed on the pair of lines undergoing the maximum angular shear strain γ (Fig. 4). The coincidence of these lines is used to

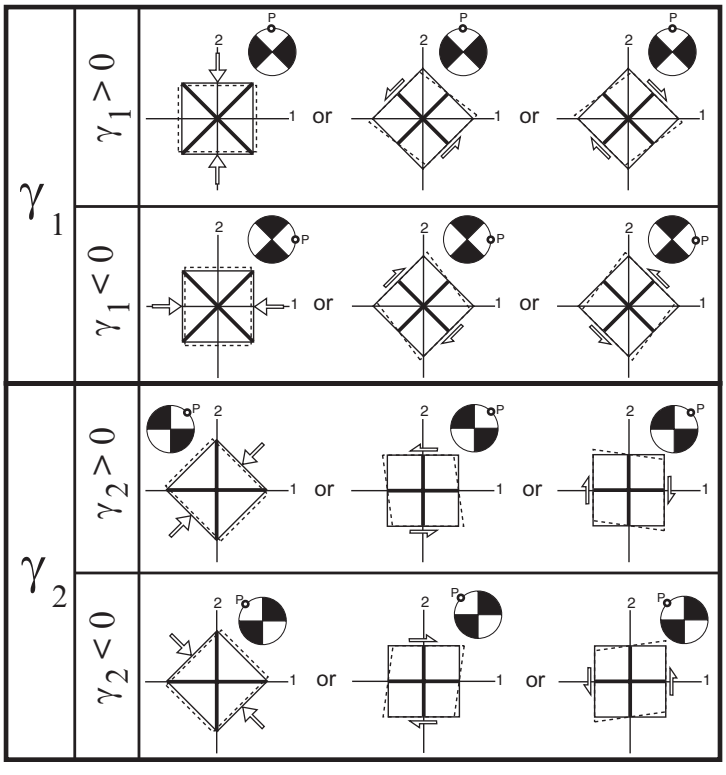

Figure 4. Interpretation of angular shear γ_1 and γ_2 with respect to focal mechanism and P-axis direction.

test the compatibility between the shortening direction deduced from the deformation of the network triangles and the direction indicated by the focal mechanisms.

When applying the method, two points of the triangulation survey have their coordinates fixed to the GPS values to scale and orient the network. Since rigid body rotation, translation and dilatation cannot be determined, as stated above, the distortion component rather than the displacement field was calculated and the values of the maximum angular shear strain rate were extracted. The maximum angular shear rates do not therefore depend on the choice of the two fixed points used for the triangulation adjustment. Calculation of the maximum angular shear strain rates assumes that the deformation pattern is continuous within the triangular finite elements of the network. For convenience, the calculations are performed using barycentric coordinates for each set of three points. It is important to check afterwards that the maximum angular shear rates for two adjacent sets of points are similar enough.

The numerical values of the constants $\partial U/\partial x$, $\partial U/\partial y$, $\partial V/\partial x$ and $\partial V/\partial y$ are determined from the displacements of the three apices of each triangle of the network.

The maximum angular shear rate or maximum shear strain rate is obtained from eq. (2), where $\gamma_1=(\partial U/\partial x-\partial V/\partial y)/T$ and $\gamma_2=(\partial U/\partial y-\partial V/\partial x)/T$, where U and V are the displacement components along the x- and y-axes, $\partial U/\partial x$, $\partial U/\partial y$, $\partial V/\partial x$ and $\partial V/\partial y$ are the displacement gradient components and T is the time span between the measurements compared.

The direction ψ of the maximum shortening rate is given by eq. (3). The maximum angular shear rates were established at the barycentre of the corresponding triangle with a bar length proportional to $\gamma\cdot$ and an orientation given by the direction α of the maximum compression direction.

Monte Carlo analysis of the error

In this analysis errors were considered to be caused only by errors in the triangulation data, which are the less accurate set of data. In order to represent the error criteria on the angular shear rates, a Monte Carlo analysis (Kasser *et al*. 1987) is used. The method of Kasser *et al*. consists of adding random noise to the observations. In a first step, random values with a normal distribution are generated, and each observation is then changed by one random value multiplied by its standard deviation scaled by the square root of the variance factor estimated from the adjustment of the initial set of observations. By adjusting one set of disturbed values, one set of disturbed maximum angular shear rates can be determined. After 50 adjustments of disturbed observations, the maximum angular shear rate is represented by a bar and the different disturbed values by a pair of points. A maximum angular shear rate is considered significant at the 66 per cent confidence level if the cluster of points representing the disturbed values does not cover all the bar (Fig. 3).

RESULTS

Fig. 3 shows a few triangles where shear strain rates are significant at the 66 per cent confidence level. This does not necessarily mean that other triangles are not deformed, just that the deformation rate is not significant enough to be measured by this method.

Triangles showing significant shear strain rates are located as follows: (1) some entirely in the Digne Nappe (triangles 1, 3, 4 and 6) and others with theirs vertices on both sides of the

frontal thrust of the Digne Nappe (triangles 5, 7, 16, 21, 22, 26, 31, 38, 39, 42); (2) in the northern Valensole Basin (triangles 25, 26, 30, 31); and (3) along the Moyenne Durance Fault (triangles 25, 30 and 40 located at the northern and southern ends of the fault). In the frontal part of the Digne Nappe, shortening directions show variations from E–W in the northern part to NNE–SSW in the central part, and no major changes in the deformation pattern can be detected between the nappe and the northern part of the Mio–Pliocene Valensole Basin (triangles 21 and 26).

An area with negligible maximum shear strain rates can be identified south of the Lure Mountain, west of the Moyenne Durance active fault. Another area, the southern Valensole Basin and the northern ranges of the Provencal structural domain, clearly shows a lack of present-day deformation (triangle 41).

INTERPRETATION

Since no major earthquake has occurred between the two epochs of measurement, this estimated deformation does not, of course, have a coseismic origin, but reflects aseismic deformation or an interseismic strain accumulation. Since a considerable part of the network is located in the Digne Nappe, which lies on a detachment zone corresponding to Triassic evaporites at shallow depth, it is therefore possible that the surface deformation estimated by the geodetic measurements differs from the deeper deformation revealed by the focal mechanisms located below the detachment (Fig. 4).

The Digne Nappe

Triangles 1, 3 and 4 (Fig. 3), located in the inner Digne Nappe, display significant maximum shear strain rates sketched as shortening axes oriented consistently between N60° and N80° and thus comparable with previous geodetic results obtained by Ferhat *et al*. (1998) in one triangle covering part of this area. These triangles indicate the existence of present-day internal deformation of the nappe. The existence of current NE–SW shortening in the inner Digne Nappe is reinforced by several data: (1) the deformation estimation performed using the REGAL continuous GPS stations (Calais *et al*., in preparation) revealed NNE–SSW to NNW–SSE shortening directions in the southern Alps and Provence; (2) a strain rate analysis performed by comparison of triangulation and GPS data also shows N–S shortening directions east of the studied network, in the southeastern continuation of the Digne Nappe, the Castellane arc, and in the Nice arcs (Calais *et al*. 2000); and (3) the present-day reverse faulting revealed by some of the focal mechanisms available in this area (Fig. 5: *M* 4.1, 19.06.84; *M* 3.8, 12.02.89; *M* 1.4, 13.11.1994 and *M* 4, 31.10.97) (Madeddu *et al*. 1996; Sue *et al*. 1999). The current NNE–SSW shortening is also consistent with microstructural investigations (Combes 1984; Lickorish & Ford 1998) that reveal both ENE–WSW and NNE–SSW directions of compression for the Mio–Pliocene period.

This deformation may be interpreted as (1) gravitational gliding of part of the nappe, its frontal thrust being at least partially locked (Fig. 6a), (2) deformation linked to the activation of a basement thrust connected to a shallow thrust in the nappe

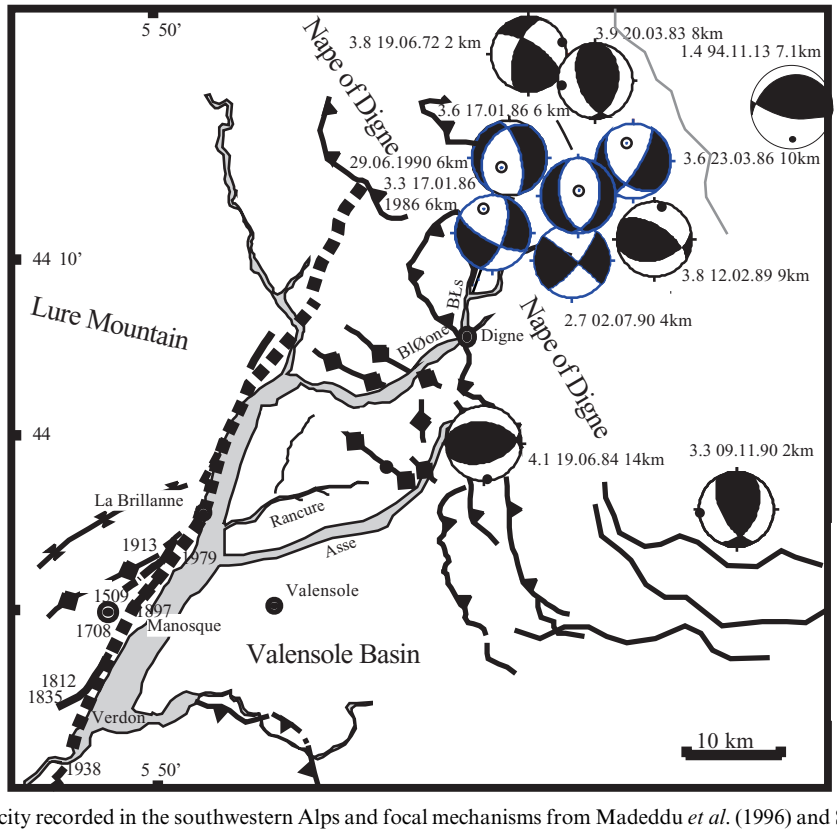

Figure 5. Historical seismicity recorded in the southwestern Alps and focal mechanisms from Madeddu *et al*. (1996) and Sue *et al*. (1999). The date or the year of occurrence of earthquakes is indicated and also the magnitude and the depth where available.

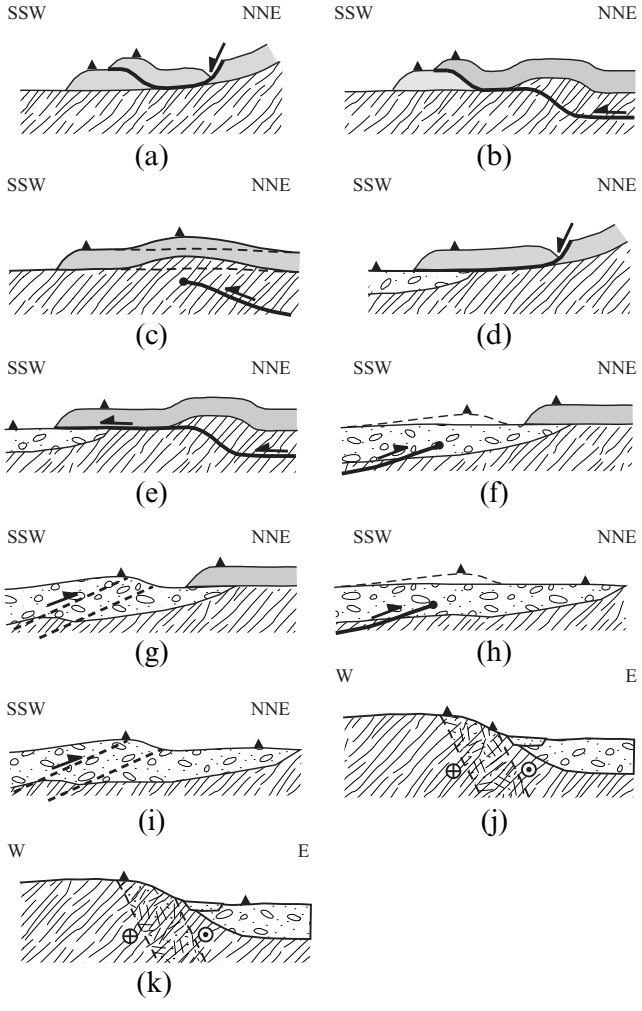

Figure 6. Possible interpretations of maximum angular shear rates. Different schemes are proposed to explain the present-day deformation of the studied area.

(Fig. 6b), and (3) interseismic strain induced by the activation of a thrust locked at depth (Fig. 6c). Hypotheses (2) and (3) are consistent with the existence of reverse faulting at depth as shown by the focal mechanisms (Fig. 4).

Triangles with their apices located on both sides of the Digne Nappe frontal thrust (Fig. 3, triangles 5, 7, 9, 16, 21, 22 and 26) exhibit significant NNE–SSW to E–W maximum shear strains. A current ENE–WSW compression around the town of Digne is confirmed by the analysis of deformation in Pliocene and Quaternary alluvial deposits (Hippolyte & Jouanne 1998). These observations can be interpreted as (1) deformation restricted to the nappe and induced by gravitational gliding of its frontal part (Fig. 6d), (2) the existence of a current NNE–SSW to NE–SW displacement on the Digne Nappe frontal thrust (triangles 5, 7 and 9) as suggested by the uplift, shown by levelling comparisons, of the Digne Nappe with respect to its foreland (Ruegg, personal communication, 1997) (Fig. 6e), or (3) deformation of the northern Valensole Basin (triangles 21 and 26), which has undergone late Miocene to Quaternary deformation (Figs 6f and g).

The progressive shortening direction changing from E–W north of the network to NNE–SSW in the central part of the network also illustrates the transition between E–W shortening as shown in the northern Subalpine Massifs and in the Jura Mountains (Jouanne *et al.* 1994, 1998; Martinod *et al.* 1996) and N–S shortening as shown in the eastern Castellane arc and in the Nice arc (Calais *et al.* 2000).

The Subalpine domain

The Subalpine fold and thrust domain (Fig. 4, triangles 13, 14, 15, 19 and 20) does not show significant shear strains, but in view of the considerable uncertainties surrounding these values, the possibility that this area is still at present absorbing minor deformation cannot be excluded.

The Valensole Basin

The northern part of the Valensole Basin is characterized by folded and faulted upper Miocene conglomerate and the southern part by subhorizontal Pliocene sediments. This north–south contrast is also observed in the deformation field: triangles with apices in the northern Valensole Basin (Fig. 4, triangles 25, 26 and 30) display significant NNE–SSW shear strain rates, while triangle 41 with one apex in the Valensole Basin and the others in the Provence Ranges does not undergo any significant deformation. This deformation may be interpreted as the activation of an aseismic thrust or shear band (Figs 6h and j) or as an interseismic strain accumulation (Fig. 6i). Unfortunately, in view of the low density of the station points in the network, the limit of the present-day deformation between the deformed northern Valensole Basin and the undeformed southern Valensole Basin near the Provence ranges cannot be accurately defined.

The Moyenne Durance Fault

The Moyenne Durance Fault shows a periodic moderate historical seismicity in its southern part (Fig. 5). From geodetic measurements a significant maximum shear strain can be estimated in three triangles with apices on both sides of the active fault (triangles 25, 30 and 40). Two of these three triangles (Fig. 4, triangles 30 and 40) show consistent NNW–SSE shortening axes that are compatible with a reverse displacement involving a small sinistral strike-slip component along the Moyenne Durance Fault. This analysis is in good agreement with the existence of at least one palaeo-earthquake characterized by a reverse sinistral strike-slip displacement of about 1 m that occurred between 27 000 and 9000 yr BP (Sébrier *et al.* 1996), which might be a coseismic displacement with a $M_w = 6.4$–6.9 earthquake. Moreover, the maximum shortening directions are also compatible with the N–S and NW–SE P-axes of two microseisms located along the southern part of the Durance Fault (Volant *et al.* 1999). The geodetic data may thus be interpreted as an elastic strain accumulation along the Moyenne Durance Fault during an interseismic period (Fig. 6j) or as the occurrence of a present-day aseismic reverse displacement with a sinistral strike-slip component along the fault zone (Fig. 6k). Triangles located just west of this zone show negligible deformation, which seems to indicate that, if this deformation reflects interseismic strain accumulation, the area undergoing this (elastic) deformation is a narrow strip a few kilometres wide. Triangle 25, displaying a NNE–SSW shear strain rate, might be independent of the present-day deformation of the Moyenne Durance Fault but is more likely to be involved in the deformation of the northern Valensole Basin. This suggests

once again that the Durance Fault zone vanishes north of the Valensole Plateau.

The Lure Mountain and the Lubéron Mountain

The western part of the network (Fig. 4, triangles 17, 24, 28, 29, 32 and 36) shows negligible and insignificant maximum shear strain rates. The most probable explanation is a lack of current tectonics as suggested by the absence of historical seismicity. Nevertheless, triangle 12 and triangles 10 and 11, affected by non-significant deformation at the 66 per cent level, may indicate north–south shortening north of the Lure Mountain with a very low deformation rate.

CONCLUSIONS

The southwestern Alps display very moderate present-day deformation located in the Digne Nappe, the northern Valensole Basin and along the Moyenne Durance Fault. In the Digne Nappe, maximum shear strain varies in terms of the directions of the shortening axes from ENE–WSW in the northern part to NNE–SSW in the southern part. Data show both internal deformation of the nappe and shear strain in the vicinity of the Digne frontal thrust. Significant shear strain rates in the northern Valensole Plateau indicate the existence of current deformation not just along the Digne Nappe frontal thrust but also in the northern part of the Valensole basin

Some data also seem to confirm present-day reverse and sinistral strike-slip movements along the Moyenne Durance Fault, which shows regular historical seismicity in its southern part. The estimated deformation may reveal the existence of an interseismic strain accumulation across the Moyenne Durance Fault zone.

ACKNOWLEDGMENTS

This paper is contribution Geofrance 3D Alpes no. 61. This work was performed with the financial and scientific support of the IPSN–CEA. Many thanks are due to the Digne 97 GPS Team: S. Roux. A. Berger, V. Fourneret, Y. Callonge, B. Opolka, C. Desbrus, N. Gurret, A. Rouge, C. Gerland, C. David, P. Vuilien, B. Danieli, C. Chaffraix and T. Thierry.

REFERENCES

Bergerat, F., 1985. Déformation cassante et champs de contraintes tertiaires dans la plate-forme européenne, *Thèse d'Etat,* University of Paris VI.

Calais, E. *et al.*, 2000. Crustal strain in the southern Alps, France, 1948–1998, *Tectonophysics,* **319,** 1–17.

Clauzon, G., 1975. Sur l'âge villafranchien du chevauchement subalpin au droit de Puimoisson (Alpes-de-Haute-Provence), *C. R. Acad. Sci. Paris,* **280,** 2433–2436.

Combes, P., 1984. La tectonique récente de la Provence occidentale: microtectonique, caractéristiques dynamiques et cinématiques, méthodologie de zonation sismotectonique. Thèse *3e cycle,* Strasbourg.

Duquenne, H., 1997. Comparison between the EGM96 model and the French quasi-geoid model, *Bull. Int. Geoid Service, DIIAR,* Politecnico di Milano, Italy, no. 6.

Duquenne, H., 1998. Grille de correction pour effectuer du nivellement par GPS, *Géomètre,* **6**.

Faucher, T., Gidon, M., Pairis, J.-L. & Mascle, G., 1988. Directions de transport au front de la Nappe de Digne (Chaînes subalpines méridionales) *C. R. Acad. Sci. Paris,* **306,** 227–230.

Feigl, K., King, W. & Jordan, T., 1990. Geodetic measurement of tectonic deformation in the Santa Maria fold and thrust belt, California, *J. geophys. Res.,* **95**(B3)**,** 2679–2699.

Ferhat, G., Feigl, K., Ritz, J.F. & Souriau, A., 1998. Geodetic measurement of tectonic deformation in the southern Alps and Provence, France, 1947–1994, *Earth planet. Sci. Lett.,* **159,** 35–46.

Frank, F.C., 1966. Deduction of earth strains from survey data, *Bull. seism. Soc. Am.,* **56,** 35–42.

Haccard, D., Beaudoin, B., Gigot, P. & Jorda, M., 1989. *Carte Géol, France (1/50 000), feuille La Javie (918),* BRGM, Orléans, France.

Hippolyte, J.-C. & Jouanne, F., 1998. L'intérêt néotectonique des mesures de déformation dans les alluvions du Pliocène-Quaternaire: exemples dans les Alpes du Sud, séminaire mouvements actuels de la surface terrestre et des massifs rocheux: mesure et interprétation, Les Houches, 74.

Jaeger, J.C., 1978. Elasticity, fracture and flow, *Science Paperback,* Chapman & Hall, London.

Jorda, M., Combes, P. & Philip, H., 1992. Tectogenèse et morphogenèse quaternaires des chaînes subalpines méridionales (région de Digne et vallée de la Bléone), *Quaternaire,* **3,** 129–135.

Jouanne, F., Ménard, G. & Jault, D., 1994. Present-day deformation of the french northwestern Alps/southern Jura mountains: comparison between historical triangulations, *Geophys. J. Int.,* **119,** 151–165.

Jouanne, F., Genaudeau, N., Ménard, G. & Darmendrail, X., 1998. Estimating current displacement fields and tectonic deformation in active mountain belts: an example from the Chartreuse massif and the Southern Jura Mountains, Western Alps, *Tectonophysics,* **296,** 403–419.

Kasser, M., Ruegg, J.C., Lesage, P., Ortlieb, L., Pagarete, J., Dutch, N., Guerero, J. & Roldan, J., 1987. Geodetic measurement of plate motion across the central Gulf of California, *Geophys. Res. Lett.,* **14,** 5–8.

Lambert, J., Levret-Albaret, A., Cushing, M. & Durouchoux, C., 1996. *Mille Ans de Séismes en France,* Ouest Editions, Presses académiques.

Lickorish, W.H. & Ford, M., 1998. Sequential restoration of the external alpine Digne Thrust system, SE France, constrained by kinematic data and syn-orogenic sediments, in *Cenozoic Foreland Basins of Western Europe,* eds Mascle, A., Puigdefabregas, C. & Fernandez, M., *Geol. Soc. Spec. Publ.,* **134,** 189–211.

Martinod, J., Jouanne, F., Taverna, J., Ménard, G., Gamond, J.F., Darmendrail, X., Notter, J.C. & Basile, C., 1996. Present-day deformation of the Dauphiné (SE France) Alpine and Subalpine Massifs, *Geophys. J. Int.,* **127,** 189–200.

Madeddu, B., Béthoux, N. & Stéphan, J.-F., 1996. Champ de contrainte post-Pliocène et déformations récentes dans les Alpes sud-occidentales, *Bull. Soc. géol. Fr.,* **167,** 797–810.

Ramsay, J.G., 1967. *Folding and Fracturing of Rocks,* McGraw-Hill, New York.

Ramsay, J.G. & Huber, M.I., 1983. *The Techniques of Modern Structural Geology, Vol. 1: Strain Analysis,* Academic Press, London.

Reilly, W.I. & Gubler, E., 1990. Crustal strain in Switzerland 1870–1970, *Geophys. J. Int.,* **103,** 251–256.

Ritz, J.-F., 1992. Tectonique récente et sismotectonique des Alpes du Sud: analyse en termes de contraintes, *Quaternaire,* **3,** 111–124.

Roure, F., Brun, J.P., Coletta, B. & Van Den Driessche, J., 1992. Geometry and kinematics of extensional structures in the alpine foreland basin of Southeastern France, *J. struct. Geol.,* **14,** 503–520.

Sébrier, M., Ghafiri, A. & Bles, J.L., 1996. Paleoseismicity in France, fault trench studies in a region of moderate seismicity, *J. Geodyn.,* **24,** 207–217.

Sue, C., Thouvenot, F., Fréchet, J. & Tricart, P., 1999. Widespread extension in the core of the western Alps revealed by earthquake analysis, *J. geophys. Res.,* **B11,** 25 611.

Terrier, M., 1991. Néotectonique de la Provence occidentale (France): vers une analyse multicritère des déformations récentes, Application à la classification des structures sismogènes, *PhD thesis,* University of Aix-Marseille I, France.

Volant, P., Berges-Thierry, C., Dervin, P., Cushing, M., Mohammadioun, G. & Matthieu, F., 1999. The south Eastern Durance Fault Permanent Network: preliminary results, *J. Seism.,* **4,** 175–189.